

Magnetic and magnetotransport properties of layered $TaCoTe_2$ single crystals

Ming Mei(梅明), Zheng Chen(陈正), Yong Nie(聂勇), Yuanyuan Wang(王园园), Xiangde Zhu(朱相德), Wei Ning(宁伟), and Mingliang Tian(田明亮)
Citation: Chin. Phys. B, 2023, 32 (**12**): 127303. DOI: 10.1088/1674-1056/acd10a
Journal homepage: http://cpb.iphy.ac.cn; http://iopscience.iop.org/cpb

What follows is a list of articles you may be interested in

Perspectives of spin-valley locking devices

Lingling Tao(陶玲玲)
Chin. Phys. B, 2023, 32 (**10**): 107306. DOI: 10.1088/1674-1056/acc809

Anisotropic plasmon dispersion and damping in multilayer 8-*Pmmn* borophene structures

Kejian Liu(刘可鉴), Jian Li(李健), Qing-Xu Li(李清旭), and Jia-Ji Zhu(朱家骥)
Chin. Phys. B, 2022, 31 (**11**): 117303. DOI: 10.1088/1674-1056/ac6b2d

Half-metallicity induced by out-of-plane electric field on phosphorene nanoribbons

Xiao-Fang Ouyang(欧阳小芳) and Lu Wang(王路)
Chin. Phys. B, 2022, 31 (**7**): 077304. DOI: 10.1088/1674-1056/ac560d

Two-dimensional topological semimetals

Xiaolong Feng(冯晓龙), Jiaojiao Zhu(朱娇娇), Weikang Wu(吴维康), and Shengyuan A. Yang(杨声远)
Chin. Phys. B, 2021, 30 (**10**): 107304. DOI: 10.1088/1674-1056/ac1f0c

Progress on 2D topological insulators and potential applications in electronic devices

Yanhui Hou(侯延辉), Teng Zhang(张腾), Jiatao Sun(孙家涛), Liwei Liu(刘立巍), Yugui Yao(姚裕贵), Yeliang Wang(王业亮)
Chin. Phys. B, 2020, 29 (**9**): 097304. DOI: 10.1088/1674-1056/aba9c5

Magnetic and magnetotransport properties of layered $TaCoTe_2$ single crystals

Ming Mei(梅明)[1,2,†], Zheng Chen(陈正)[1,†], Yong Nie(聂勇)[1,2], Yuanyuan Wang(王园园)[1,2], Xiangde Zhu(朱相德)[1,‡], Wei Ning(宁伟)[1,§], and Mingliang Tian(田明亮)[1,3]

[1] *Anhui Key Laboratory of Condensed Matter Physics at Extreme Conditions, High Magnetic Field Laboratory, HFIPS, Anhui, Chinese Academy of Sciences, Hefei* 230031, *China*

[2] *Department of Physics, University of Science and Technology of China, Hefei* 230031, *China*

[3] *School of Physics, Anhui University, Hefei* 230601, *China*

(Received 13 March 2023; revised manuscript received 28 April 2023; accepted manuscript online 28 April 2023)

We present the synthesis of $TaCoTe_2$ single crystals and a systematic investigation of the physical properties of bulk crystals and thin flakes. The crystal shows a semiconducting behavior with temperature decreasing from room temperature and turns to a metallic behavior below 38 K. When the magnetic field is applied, the temperature-dependent resistivity curves show an upturn below 10 K. Furthermore, we find that the $TaCoTe_2$ single crystal can be easily exfoliated from the bulk crystal by the micromechanical exfoliation method. Our measurements suggest that the nanoflakes have properties similar to those of the bulk crystal when the thickness is lowered to 18 nm.

Keywords: two-dimensional materials, magnetism, electronic transport, nanoflakes

PACS: 73.63.–b, 68.65.–k, 75.70.Ak, 75.75.Cd **DOI:** 10.1088/1674-1056/acd10a

1. Introduction

Since the discovery of graphene, two-dimensional (2D) materials have proved to be a fertile ground to explore novel electrical,[1–4] optical,[5–7] mechanical,[8,9] and magnetic properties.[10–13] In 2D materials, it has been confirmed that the decrease in the crystal dimension makes it sensitive to carrier concentration, magnetic field, pressure and electric field, and novel phenomena that are different from the bulk crystal can be observed, such as the observation of the quantum Hall effect in graphene,[14] the strongly thickness-dependent metallic to semiconductor, charge density wave, or superconducting phases in transition metal dichalcogenides,[15,16] the layer-dependent ferromagnetism in 2D magnetic materials,[17,18] the observation of the quantum anomalous Hall effect in few-layer $MnBi_2Te_4$,[19] and the enhancement of a weak-antilocalization signature in Nb_3SiTe_6.[20] During the past decade, a number of important potential applications have been proven in 2D materials.[15,21–28] Many new 2D materials have been predicted that are worth further experimental studies.

Theoretic investigation has predicted that the Dirac points can be stabilized in 2D materials. However, it remains a challenge to identify concrete 2D materials that host such magnetic Dirac points. Recently, the layered ternary telluride $TaCoTe_2$ was predicted to be a new topological semimetal.[29] It is suggested that the monolayer $TaCoTe_2$ is stable with an antiferromagnetic (AFM) ground state. It hosts a pair of 2D AFM Dirac points on the Fermi level in the absence of spin–orbit coupling (SOC) and emerged another pair of magnetic Dirac points below the Fermi level when SOC is included. An angle-resolved photoelectron spectroscopy study reported the experimental signature of topological Dirac antiferromagnetism in this material.[30] However, the physics properties of this material have not been well studied. In this work, we have synthesized high-quality single crystal $TaCoTe_2$ and performed a detailed investigation into both the bulk crystals through magnetization and magnetotransport measurements. We also obtained nanoflakes by the Scotch tape-based micromechanical exfoliation method and fabricated nanodevices based on these nanoflakes. We found that when the thickness is reduced to 18 nm, the crystal shows the same properties as the bulk crystal.

2. Experiment

2.1. Crystal growth and nanodevice fabrication

$TaCoTe_2$ single crystals were grown by the chemical vapor transport (CVT) method using $TeCl_4$ as a transport agent. Stoichiometric elemental agents Ta (powder), Co (powder), and Te (chunk) were mixed and sealed in a vacuumed silica tube. The tube was 20 cm in length and placed in a two-zone furnace. The transport was carried out in the temperature gradient of 930 °C to 850 °C for 7 days. Then the furnace was cooled naturally to room temperature after the reaction. Shiny black plate-like $TaCoTe_2$ single crystals were collected

†These authors contributed equally to this work.

‡Corresponding author. E-mail: xdzhu@hmfl.ac.cn

§Corresponding author. E-mail: ningwei@hmfl.ac.cn

© 2023 Chinese Physical Society and IOP Publishing Ltd

at the cold end. $TaCoTe_2$ thin flakes with different thicknesses were obtained by mechanically exfoliating the bulk crystal, followed by directly transferring them onto Si/SiO_2 substrate. Hall-bar devices were fabricated by standard electron-beam lithography followed by an Au (80 nm)/Ti (10 nm) evaporation and a liftoff process.

2.2. Material characterization

X-ray diffraction (XRD) was used to determine the structure of the as-grown single crystals. The XRD data were obtained at room temperature on a Rigaku-TTR3 (Cu $K\alpha$ radiation, $\lambda = 1.5418$ Å) operated at 20 kV voltage and 4 mA current with a flat single-crystal specimen mounted on the sample holder in a reflection mode (step size = 0.02°). The composition analysis of single crystals was done by an energy dispersive spectroscopy (EDS) upon a dual beam system (Helios nanolab600i), operated at 20 kV voltage and 0.17 nA current. The resistivity measurement was measured by the four-probe method and was carried out by a physical properties measurement system (PPMS-14T, QD Inc.). Magnetization measurement was performed upon a magnetic properties measurement system (MPMS3-7T, QD Inc.). Electron beam lithography was used to prepare devices and was also performed upon a dual beam system (Helios nanolab600i). The measurement of the sample thickness was performed using an atomic force microscope (NX10, PARK Inc.).

3. Results and discussion

In previous work,[31] polycrystalline XRD has determined the structure of the $TaCoTe_2$. $TaCoTe_2$ has crystallized in space group $P2_1/c$ (No. 14) with $a = 8.1524$ Å, $b = 6.2649(4)$ Å, $c = 7.7945$ Å, and $\alpha = 116.789°$. The crystal structure of $TaCoTe_2$ is shown in Figs. 1(a) and 1(b). As illustrated, the crystal has a layered structure aligned along the a-axis. Figure 1(c) depicts the room temperature XRD pattern of our single crystal. All the peaks can be indexed as (L00) reflections. The inset of Fig. 1(c) show an optical image of an as-grown $TaCoTe_2$ single crystal. This indicates that the largest naturally grown surface of the crystals belongs to the bc plane. As shown in Fig. 1(d), the obtained chemical composition from the EDS of three elements Ta, Co, and Te is 1:1:2.

Figure 2(a) depicts the temperature-dependent magnetization curves (M–T) of single crystal $TaCoTe_2$ under field-cooled (FC) and the zero-field-cooled (ZFC) modes, with magnetic field $H = 1$ T applied along the a-axis ($H\|a$-axis) and parallel to the bc plane ($H\|bc$ plane), respectively. It can be found that the M–T curves of both the FC and ZFC modes almost overlap at low temperature with the magnetic field applied parallel to the bc plane, while the two curves are not coincident at a high temperature range. Figure 2(b) shows the magnetic-field dependent magnetization at different temperatures at the $B\|bc$ plane. When the field is applied along the a-axis, it exhibits similar magnetic behavior at low temperature range. While at a high temperature range, a rapid increase in magnetization can be observed with temperature decreasing and a broad peak appears at about 250 K. DFT calculations suggest this compound should be an AFM material; thus, the peak at 250 K might be a signature magnetic ordering transition related to the predicted AFM order.[30] However, the magnetic moment is small and local lattice defects can also induce the presence of magnetization, especially at low temperature range. Further measurements are required to study the magnetic properties of $TaCoTe_2$.

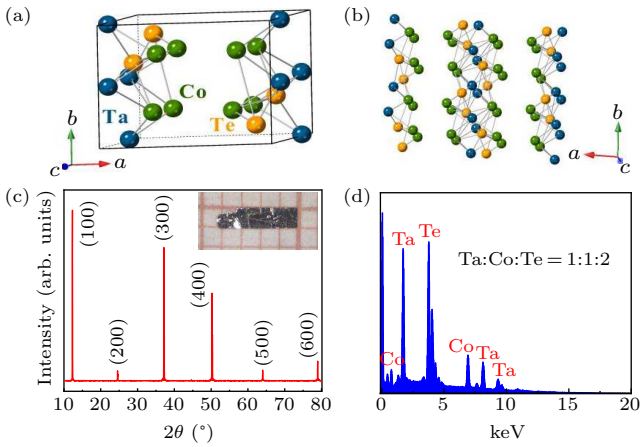


Fig. 1. (a) Schematic of a unit cell of $TaCoTe_2$ (inside solid line). (b) A layered structure of $TaCoTe_2$ that is aligned parallel to the a-axis (space group $P2_1/c$). (c) Single-crystal XRD results along the (L00) plane for $TaCoTe_2$. The inset shows an optical image of a typical as-grown $TaCoTe_2$ single crystal. (d) Typical EDS data collected on a flat clean surface of crystal showing elemental composition.

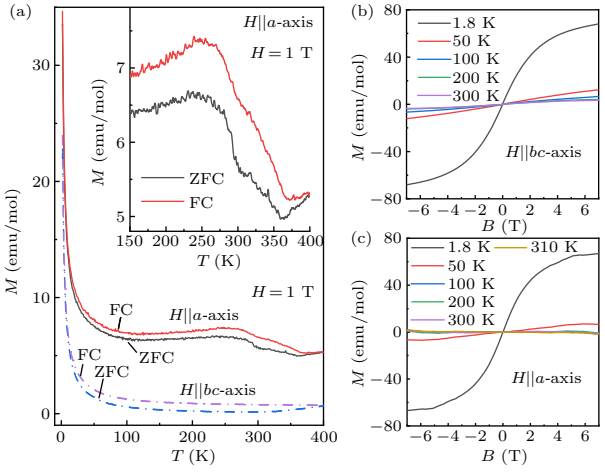


Fig. 2. (a) Temperature-dependent magnetization as function of temperature at $H = 1$ T with H applied along the a-axis (solid lines) and parallel to the bc plane (dotted lines). The inset shows the enlargement area above 150 K. (b) and (c) The magnetic-field dependent magnetization at different temperatures for the $H\|bc$ plane and a-axis, respectively.

Figure 3(a) shows the temperature-dependent resistivity ρ of bulk crystal measured with the current applied parallel to the bc plane. The resistivity ρ exhibits a semiconducting

behavior at high temperature range. As the temperature decreases, it shows a semiconducting to metallic transition with a broad peak around 38 K. When the magnetic field is applied, the curves show an upturn at low temperature. Figure 3(b) shows R–T curves for a nanodevice with thickness $d = 40$ nm. It exhibits behavior similar to that of the bulk crystal, except the temperature of the peak is a little lower than that of the bulk crystal, i.e., at 32 K. In two samples, the peak moves slightly to lower temperatures under magnetic fields. The upturn behavior is more obvious in the nanodevice. It can be expected that the resistivity may turn fully to semiconductor behavior when the magnetic field is high enough. Similar nonmetallic transport has been observed in the work,[30] which showed that the $TaCoTe_2$ crystal shows an even broader around 50 K.

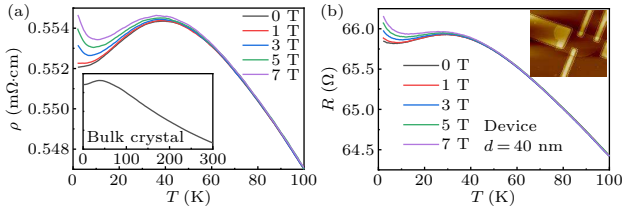


Fig. 3. (a) Temperature-dependent resistivity ρ measured with the current applied parallel to the bc plane for bulk crystal. The inset shows a ρ–T curve for the whole temperature range from 2 K–300 K. (b) Temperature-dependent resistivity ρ of a nanodevice with thickness $d = 40$ nm under different magnetic fields. The inset shows an image of a nanodevice obtained with AFM.

Figure 4(a) shows temperature-dependent MR, defined as $\mathrm{MR}(\%) = [R(B) - R(0)]/R(0) \times 100\%$, of bulk crystal with magnetic field applied along the a-axis. The value positive MR is 0.625% at 2 K at 9 T. With an increase in temperature, it reduces to about 0.05% at 40 K, 9 T. As displayed in Fig. 4(b), the MR behavior with the $H \| bc$ plane at a different temperature is almost the same as the $H \| a$-axis, suggesting a weak anisotropy between the two directions. Figures 4(c) and 4(d) show MR behavior of the nanodevice at $d = 40$ nm, measured at different temperatures with the $H \| bc$ plane and $H \| a$-axis, respectively. The value of MR is 0.61% at 2 K and 0.045% at 40 K at 9 T. Obviously, the magnetotransport property is the same as bulk crystal when the thickness is lowered down to 40 nm.

In order to further investigate the physical properties, we fabricated a nanodevice to even lower thickness. Figure 5(a) shows the ρ–T curves of the bulk crystal and three nanodevices with different thicknesses, i.e., $d = 40$ nm, 25 nm, and 18 nm for samples S1, S2, and S3, respectively. The ρ–T curves are shifted for clarify. Similar temperature dependence resistivity of all four samples can be observed. The temperature of the transition from semiconductor to metal moved to a lower temperature gradually, as indicated by the arrow. Figure 5(b) presents the MR behavior at $t = 2$ K for the three samples. All the samples exhibit similar unsaturated linear MR behavior, which indicates that the physical properties remain nearly the same even when the thickness is lowered to 18 nm. To further explore the predicted AFM behavior in monolayer $TaCoTe_2$, further work on nanoflakes with lower thickness is required.

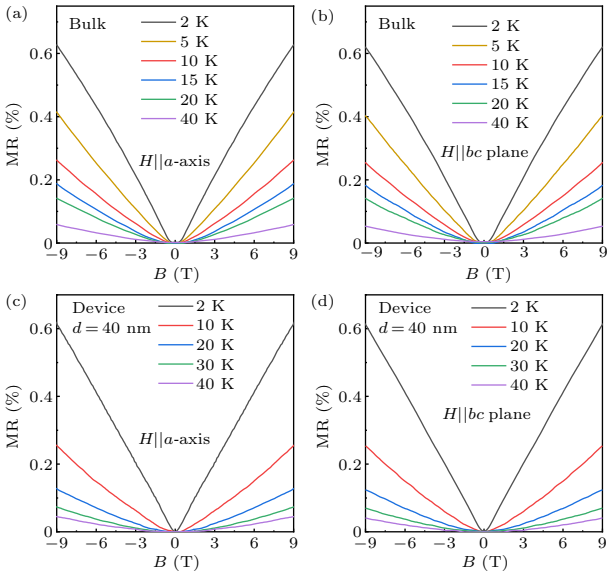


Fig. 4. (a) The MR as a function of magnetic field measured at different temperatures with H applied along the a-axis for bulk crystal. (b) Single crystal: the MR as a function of magnetic field measured at different temperatures with the $H \| bc$ plane for bulk crystal. (c) The MR as function of magnetic field measured at different temperatures with $H \| a$-axis for sample S1 ($d = 40$ nm). (d) The MR as function of magnetic field measured at different temperatures with the $H \| bc$ plane for sample S1 ($d = 40$ nm).

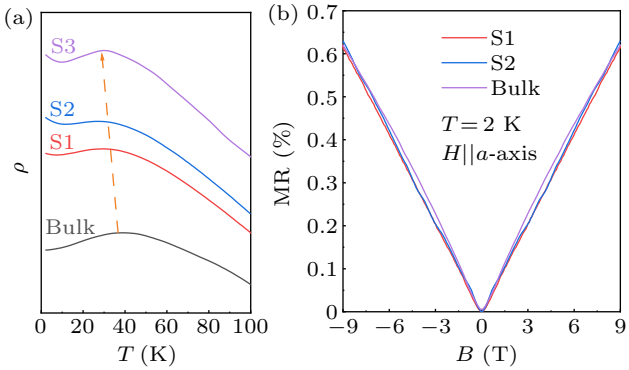


Fig. 5. (a) Temperature-dependent resistivity ρ of different samples measured with the current applied parallel to the bc plane. The curves of different samples are shifted for clarify. (b) The MR of different samples as a function of magnetic field measured at 2 K with the magnetic field applied along the a-axis.

We note that upturn behavior in resistivity below 10 K has been observed in other materials. A possible reason is the Kondo effect.[32] However, the applied magnetic field could suppress the upturn. This is not the case in our work and thus this cause could be ruled out. Another reason is the existence of a metallic surface state in the crystals. The broad hump of the temperature-dependent resistance was then considered to be the competition of the conductivity between the surface state and the bulk.[33] When the temperature decreases, the contribution of the surface conductivity dominates the transport and leads to the downturn in the R–T curves. However, in

this case, the upturn behavior in thinner samples at low temperature should not appear due to the enhanced surface conductivity. This is not consistent with our observation and thus the existence of a metallic surface state is also not the origin of the upturn at the low temperature region. We will aim to get more information on these observations in our future work.

4. Conclusion

In summary, we have successfully synthesized layered $TaCoTe_2$ crystals using the CVT method. We performed a detailed study of magnetic and magnetotransport properties on both bulk crystal and nanosheets with thickness down to 18 nm. The bulk $TaCoTe_2$ shows magnetic ordering even at room temperature. The temperature-dependent resistivity of $TaCoTe_2$ shows a transition from semiconductor to metal near 38 K. Comparing the magnetotransport behavior of samples with different thicknesses, we found that the magnetotransport properties of bulk crystal and the nanoflakes even down to 18 nm are the same. To further explore the predicted 2D Dirac AFM behavior, nanoflakes with even lower thicknesses are needed.

Acknowledgments

Project supported by the National Key Research and Development Program of China (Grant No. 2021YFA1600201), the National Natural Science Foundation of China (Grant Nos. U19A2093, U2032214, and U2032163), Collaborative Innovation Program of Hefei Science Center, CAS (Grant No. 2019HSC-CIP 001), Youth Innovation Promotion Association of CAS (Grant No. 2021117), the HFIPS Director's Fund (Grant No. YZJJQY202304), and the CASHIPS Director's Fund (Grant No. E26MMG71131). A portion of this work was supported by the High Magnetic Field Laboratory of Anhui Province.

References

[1] Kim S, Konar A, Hwang W S, Lee J H, Lee J, Yang J, Jung C, Kim H, Yoo J B and Choi J Y 2012 *Nat. Commun.* **3** 1011
[2] Radisavljevic B and Kis A 2013 *Nat. Mater.* **12** 815
[3] Wang H, Xu M and Zheng R 2020 *Acta Phys. Sin.* **69** 017301 (in Chinese)
[4] Qin M S, Zhu P F, Ye X G, Xu W Z, Song Z H, Liang J, Liu K and Liao Z M 2021 *Chin. Phys. Lett.* **38** 017301
[5] Zeng H and Cui X 2015 *Chem. Soc. Rev.* **44** 2629
[6] Tran K, Moody G, Wu F, Lu X, Choi J, Kim K, Rai A, Sanchez D A, Quan J and Singh A 2019 *Nature* **567** 71
[7] Wang C, Liu J and Zhang H 2019 *Acta Phys. Sin.* **68** 188101 (in Chinese)
[8] Cheng R, Jiang S, Chen Y, Liu Y, Weiss N, Cheng H C, Wu H, Huang Y and Duan X 2014 *Nat. Commun.* **5** 1
[9] Myny K 2018 *Nat. Electron.* **1** 30
[10] Huang B, Clark G, Navarro-Moratalla E, Klein D R, Cheng R, Seyler K L, Zhong D, Schmidgall E, McGuire M A and Cobden D H 2017 *Nature* **546** 270
[11] Klein D R, MacNeill D, Lado J L, Soriano D, Navarro-Moratalla E, Watanabe K, Taniguchi T, Manni S, Canfield P and Fernández-Rossier J 2018 *Science* **360** 1218
[12] Yu X Y, Feng H L, Gu G X, Liu Y H, Li Z L, Xu T S and Li Y Q 2019 *Acta Phys. Sin.* **68** 247201 (in Chinese)
[13] Hao Y, Gu Y, Gu Y, Feng E, Cao H, Chi S, Wu H and Zhao J 2021 *Chin. Phys. Lett.* **38** 096101
[14] Zhang Y, Tan Y W, Stormer H L and Kim P 2005 *Nature* **438** 201
[15] Wang Q H, Kalantar-Zadeh K, Kis A, Coleman J N and Strano M S 2012 *Nat. Nanotechnol.* **7** 699
[16] Wang H, Huang X, Lin J, Cui J, Chen Y, Zhu C, Liu F, Zeng Q, Zhou J and Yu P 2017 *Nat. Commun.* **8** 394
[17] Huang B, Clark G, Navarro-Moratalla E, Klein D R, Cheng R, Seyler K L, Zhong D, Schmidgall E, McGuire M A, Cobden D H, Yao W, Xiao D, Jarillo-Herrero P and Xu X 2017 *Nature* **546** 270
[18] Fei Z, Huang B, Malinowski P, Wang W, Song T, Sanchez J, Yao W, Xiao D, Zhu X, May A F, Wu W, Cobden D H, Chu J H and Xu X 2018 *Nat. Mater.* **17** 778
[19] Deng Y, Yu Y, Shi M Z, Guo Z, Xu Z, Wang J, Chen X H and Zhang Y 2020 *Science* **367** 895
[20] Hu J, Liu X, Yue C L, Liu J Y, Zhu H W, He J B, Wei J, Mao Z Q, Antipina L Y, Popov Z I, Sorokin P B, Liu T J, Adams P W, Radmanesh S M A, Spinu L, Ji H and Natelson D 2015 *Nat. Phys.* **11** 471
[21] Akinwande D, Petrone N and Hone J 2014 *Nat. Commun.* **5** 5678
[22] Lin Z, Liu Y, Halim U, Ding M, Liu Y, Wang Y, Jia C, Chen P, Duan X and Wang C 2018 *Nature* **562** 254
[23] Mak K F and Shan J 2016 *Nat. Photonics* **10** 216
[24] Baugher B W, Churchill H O, Yang Y and Jarillo-Herrero P 2014 *Nat. Nanotechnol.* **9** 262
[25] Zhong D, Seyler K L, Linpeng X, Cheng R, Sivadas N, Huang B, Schmidgall E, Taniguchi T, Watanabe K and McGuire M A 2017 *Sci. Adv.* **3** e1603113
[26] Jiang S, Li L, Wang Z, Shan J and Mak K F 2019 *Nat. Electron.* **2** 159
[27] Lin X, Yang W, Wang K L and Zhao W 2019 *Nat. Electron.* **2** 274
[28] Chen Y, Liu R, Chen Y, Yuan X, Ning J, Zhang C, Chen L, Wang P, He L, Zhang R, Xu Y and Wang X 2021 *Chin. Phys. Lett.* **38** 017101
[29] Li S, Liu Y, Yu Z M, Jiao Y, Guan S, Sheng X L, Yao Y and Yang S A 2019 *Phys. Rev. B* **100** 205102
[30] Mazzola F, Ghosh B, Fujii J, Acharya G, Mondal D, Rossi G, Bansil A, Farias D, Hu J, Agarwal A, Politano A and Vobornik I 2023 *Nano Lett.* **23** 902
[31] Li J, McCulley F, McDonnell S L, Masciocchi N, Proserpio D M and Sironi A 1993 *Inorg. Chem.* **32** 4829
[32] Wang Y, Xie C, Li J, Du Z, Cao L, Han Y, Zu L, Zhang H, Zhu H, Zhang X, Xiong Y and Zhao W 2021 *Phys. Rev. B* **103** 174418
[33] Ning W, Du H, Kong F, Yang J, Han Y, Tian M and Zhang Y 2013 *Sci. Rep.* **3** 1